Short Article
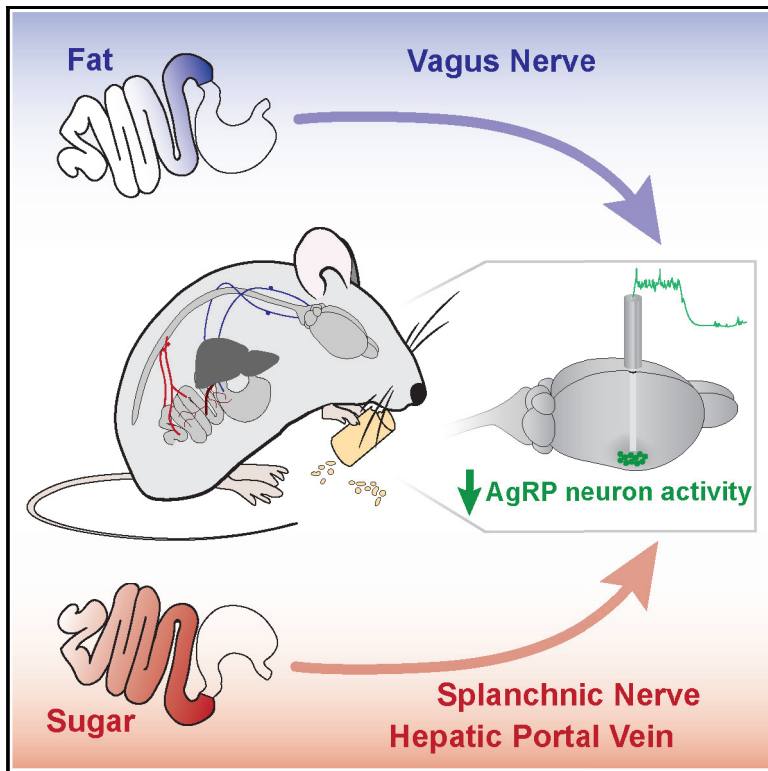
Hypothalamic detection of macronutrients via multiple gut-brain pathways

Graphical Abstract

Authors

Nitsan Goldstein, Aaron D. McKnight, Jamie R.E. Carty, Myrtha Arnold, J. Nicholas Betley, Amber L. Alhadeff

Correspondence

jnbetley@sas.upenn.edu (J.N.B.), aalhadeff@monell.org (A.L.A.)

In Brief

Macronutrients in food change hunger levels by influencing neural activity in the brain. Goldstein et al. show that fat and sugar engage distinct gut-brain pathways—using vagal and spinal/hepatic portal signaling, respectively—to reduce activity in hypothalamic hunger neurons.

Highlights

- Different macronutrients engage distinct gut-AgRP pathways

- Fat, but not glucose, inhibits AgRP neuron activity through vagal signaling

- Glucose inhibits AgRP neuron activity through spinal afferent signaling

- Intestinal and hepatic portal SGLT1 mediates gut-AgRP glucose sensing

CellPress

Cell Metabolism

CellPress

Short Article

Hypothalamic detection of macronutrients via multiple gut-brain pathways

Nitsan Goldstein,[1] Aaron D. McKnight,[2,3,5] Jamie R.E. Carty,[1,5] Myrtha Arnold,[4] J. Nicholas Betley,[1,*] and Amber L. Alhadeff[2,3,6,*]

[1]Department of Biology, University of Pennsylvania, Philadelphia, PA 19104, USA
[2]Monell Chemical Senses Center, Philadelphia, PA 19104, USA
[3]Department of Neuroscience, University of Pennsylvania, Philadelphia, PA 19104, USA
[4]Department of Health Sciences and Technology, ETH Zurich, Switzerland
[5]These authors contributed equally
[6]Lead contact
*Correspondence: jnbetley@sas.upenn.edu (J.N.B.), aalhadeff@monell.org (A.L.A.)
https://doi.org/10.1016/j.cmet.2020.12.018

SUMMARY

Food intake is tightly regulated by complex and coordinated gut-brain interactions. Nutrients rapidly modulate activity in key populations of hypothalamic neurons that regulate food intake, including hunger-sensitive agouti-related protein (AgRP)-expressing neurons. Because individual macronutrients engage specific receptors in the gut to communicate with the brain, we reasoned that macronutrients may utilize different pathways to reduce activity in AgRP neurons. Here, we revealed that AgRP neuron activity in hungry mice is inhibited by site-specific intestinal detection of different macronutrients. We showed that vagal gut-brain signaling is required for AgRP neuron inhibition by fat. In contrast, spinal gut-brain signaling relays the presence of intestinal glucose. Further, we identified glucose sensors in the intestine and hepatic portal vein that mediate glucose-dependent AgRP neuron inhibition. Therefore, distinct pathways are activated by individual macronutrients to inhibit AgRP neuron activity.

INTRODUCTION

Maintaining balance between nutrient need and consumption requires exquisite coordination between the gut and the brain. While gut effects on satiation centers are well characterized (Chambers et al., 2013; Johnstone et al., 2006; Olson et al., 1993; Phifer and Berthoud, 1998; Tsurugizawa et al., 2008), it is also important to understand how gut signals influence neural activity in key neuron populations that drive feeding. Therefore, we aimed to determine the gut-brain pathways that reduce neural activity in agouti-related protein (AgRP)-expressing neurons, a hypothalamic neuron population highly active during hunger that promotes robust feeding behavior (Aponte et al., 2011; Betley et al., 2015; Chen et al., 2015; Krashes et al., 2011; Mandelblat-Cerf et al., 2015; Takahashi and Cone, 2005).

Direct nutrient infusions into the gut cause rapid and sustained reductions in AgRP neuron activity (Beutler et al., 2017; Su et al., 2017). However, the peripheral pathways through which nutrients in the gut transmit signals to AgRP neurons remain largely unknown. Multiple pathways for gut-brain communication have been described. For example, vagal and spinal afferents rapidly transmit signals from the gut to the brain (Berthoud et al., 2004; Brookes et al., 2013; Fox et al., 2000; Williams et al., 2016). Humoral signals (e.g., satiation signals) released from the gut upon food detection signal the brain through paracrine action on vagal afferents or circulation (Batterham et al., 2002; Lutz, 2006; Moran et al., 2001). Nutrients can also enter the circulation and inhibit food intake through portal mesenteric signaling or direct action in the brain (Levin et al., 1999; Tordoff and Friedman, 1986; Tordoff et al., 1989; Zhang et al., 2018). Interestingly, there are differences in how distinct macronutrients (i.e., fat, carbohydrate, and protein) engage these pathways to communicate with the brain (de Araujo et al., 2020; Qu et al., 2019; Woltman and Reidelberger, 1995; Yox et al., 1991).

Where along the gastrointestinal tract are nutrients detected and relayed to AgRP neurons? And what are the peripheral pathways through which different macronutrients in the gut relay signals to the brain to modulate AgRP neuron activity? To address these questions, we examined how different nutrients inhibit AgRP neuron activity to influence feeding behavior. We found that AgRP neuron activity changes depend on the type of macronutrient and intestinal site of detection. Fat, but not sugar, required vagal signaling to inhibit AgRP neuron activity. Further, spinal afferents activated by glucose sensors in the intestine and hepatic portal vein were sufficient to inhibit AgRP neuron activity. Finally, we demonstrated that AgRP neuron activity reductions by post-ingestive nutrients can accurately predict feeding behavior, regardless of where they are detected. Together, this work reveals that nutrients engage multiple gut-brain pathways to inhibit AgRP neurons and maintain energy homeostasis.

(legend on next page)

Cell Metabolism
Short Article

CellPress
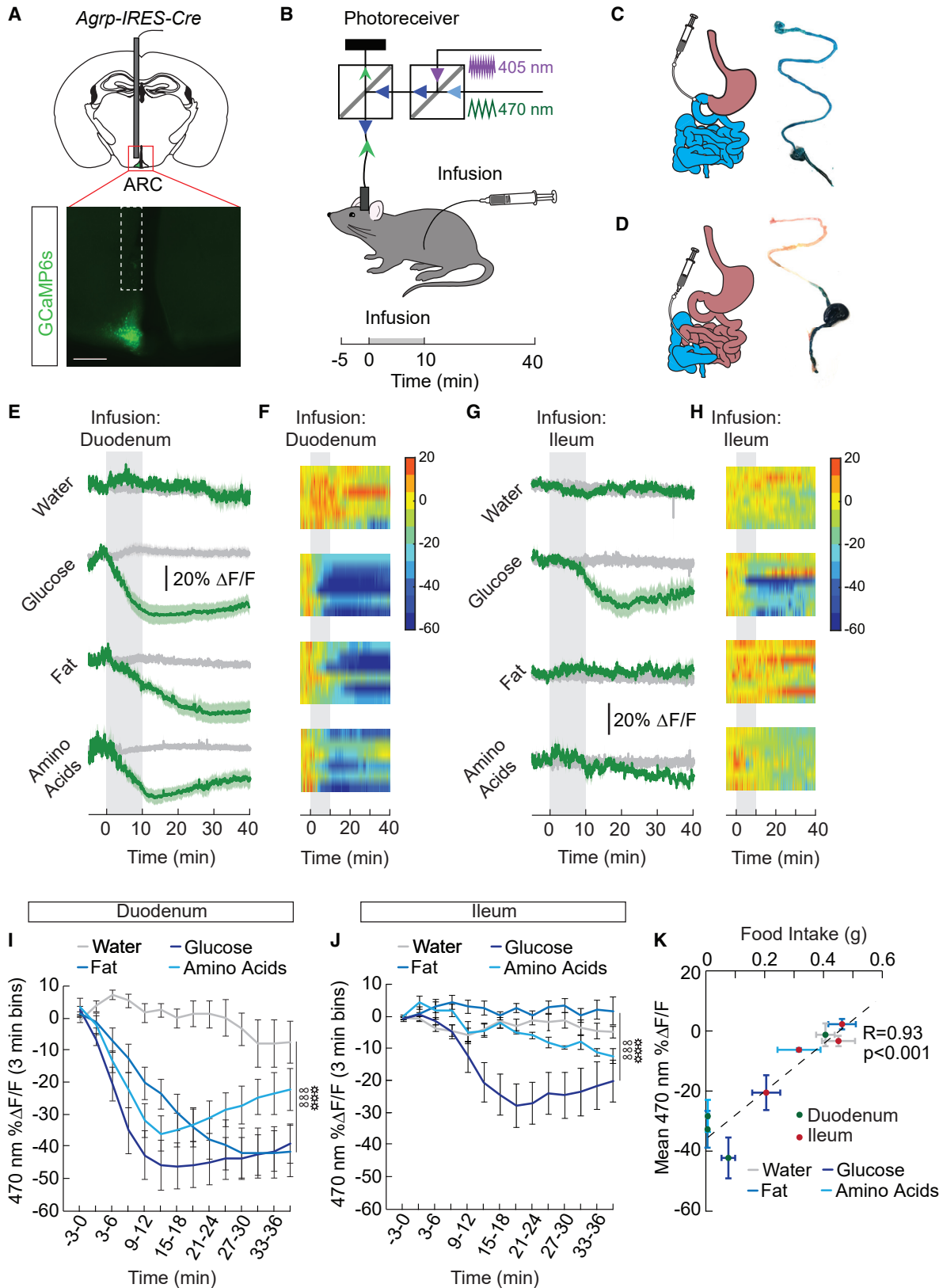
RESULTS

Site-specific detection of macronutrients in the intestine by AgRP neurons

Our previous work demonstrated that individual macronutrients infused into the stomach inhibit AgRP neuron activity in hungry mice (Beutler et al., 2017; Su et al., 2017). The small intestine is the primary site of nutrient absorption (Breen et al., 2013), and distinct macronutrients engage different cells, receptors, and transporters along the gut epithelium. To determine the sites along the small intestine where nutrients are detected and relayed to feeding centers in the brain, we monitored AgRP neuron activity while infusing nutrients in either the proximal or distal small intestine. We engineered mice to express the genetically encoded calcium indicator, GCaMP6s, in AgRP neurons (Figure 1A) and monitored neural activity during intestinal infusion of nutrients (Figure 1B). We catheterized the proximal (duodenal) and distal (ileal) small intestine and confirmed our ability to restrict infusions to sites downstream of the catheter (Figures 1C and 1D). Infusion of each macronutrient (fat [Intralipid], carbohydrate [glucose], and amino acids [Proteinex], 1 mL/10 min) (Su et al., 2017) into the duodenum significantly reduced AgRP neuron activity (Figures 1E, 1F, and 1I). We performed a dose response of these macronutrients delivered to the duodenum (Figures S1A–S1C) and identified doses (kcal) that led to similar reductions in AgRP neuron activity (Figures S1F–S1H). For each macronutrient, the AgRP neuron response to duodenal infusion was similar in magnitude to gastric infusion (Figure S2), suggesting that the stomach does not play an integral role in mediating AgRP neuron activity changes. In contrast to duodenal infusions where all macronutrients are sufficient to inhibit AgRP neurons, only infusion of glucose into the ileum significantly reduced AgRP neuron activity (Figures 1G, 1H, and 1J). These data demonstrate that duodenal sensing is required for maximal AgRP neuron activity reductions by all macronutrients, but that glucose infusions throughout the small intestine are sufficient to signal AgRP neurons.

To explore how site-specific differences in intestinal nutrient detection relate to behavior, we monitored food intake in food-restricted mice following duodenal or ileal infusion of different nutrients (Figure S1D). Infusion of glucose, fat, or amino acids into the duodenum significantly inhibited food intake (Figure S1E). In contrast, ileal infusion of glucose, but not fat or amino acids, inhibited food intake (Figure S3A), and the food intake suppression following duodenal infusion is more robust than intake suppression following ileal infusion (Figures S3D–S3F). The ability of macronutrients to inhibit food intake is similar to the inhibitory effects on AgRP neuron activity (Figures S1F–S1H, S2, S3B, and S3C). In fact, across experiments, the inhibition of AgRP neuron activity by intestinal macronutrients was almost perfectly correlated with food intake reductions (Figure 1K). Therefore, when postingestive effects of nutrients are isolated, AgRP neuron activity inhibition is a remarkable predictor of feeding behavior.

While there was a robust suppression of food intake and AgRP neuron activity in response to duodenal fat, there was no suppression in response to ileal fat (Figures 1G, 1J, and S3A). We first tested if fat digestion was required for AgRP neuron inhibition by fat. High doses of the lipase inhibitor, orlistat, eliminated the effect of Intralipid on both food intake and AgRP neuron activity (Figures S4A–S4D). We next explored whether the type of fat (triglyceride versus free fatty acid) influences effects on food intake and AgRP neuron activity. Intralipid is a fat emulsion composed primarily of triglycerides, like most commonly ingested fats (Bell et al., 1997; Castelli, 1986), which are broken down into fatty acids. Therefore, we infused oleic acid, a free fatty acid component of Intralipid, into the intestine to determine if triglyceride breakdown products can influence food intake or AgRP neuron activity. Consistent with previous work (Woltman and Reidelberger, 1995), oleic acid infusion into the duodenum or ileum inhibited food intake (Figure S4E). In contrast, oleic acid infused into the duodenum, but not the ileum, inhibited AgRP neuron activity (Figures S4F–S4H). These data support our finding that the duodenum is the essential detection site for the effects of fats on AgRP neuron activity.

Vagal-dependent detection of fat, but not glucose, by hypothalamic neurons

We next explored the gut-brain pathways used to inhibit AgRP neuron activity. To examine the contribution of vagal signaling

---

Figure 1. Site-specific detection of macronutrients in the intestine by AgRP neurons

(A) Representative image showing GCaMP6s expression in AgRP neurons of *AgRP-IRES-Cre* mice. Scale bar, 200 μm.

(B) Schematic showing the dual-wavelength fiber photometry setup used to monitor AgRP neuron activity during infusions into the intestine. Infusates were delivered over 10 min (1 mL, 0.1 mL/min).

(C) Schematic and representative image of a duodenal infusion.

(D) Schematic and representative image of an ileal infusion.

(E) Average ΔF/F of GCaMP6s signals in AgRP neurons of food-restricted mice with intra-duodenal (ID) infusions of water, glucose (2/3 kcal), fat (1 kcal), and amino acids (1 kcal) (n = 6/group). Signals are aligned to the start of the infusion. Green, 470-nm calcium signal; gray, 405-nm control signal. Dark lines represent means and lighter shaded areas represent SEM.

(F) Heatmaps reporting ΔF/F of the 470-nm signal of the recordings in individual mice in (E).

(G) Average ΔF/F of GCaMP6s signals in AgRP neurons of food-restricted mice with intra-ileal (II) infusions of water, glucose (2/3 kcal), fat (1 kcal), and amino acids (1 kcal) (n = 6–8/group).

(H) Heatmaps reporting ΔF/F of the 470-nm signal of the recordings in individual mice in (G).

(I) Mean ΔF/F of the 470-nm signal (3-min bins) in AgRP neurons with ID infusions of macronutrients in (E) (n = 6/group, two-way repeated-measures ANOVA, p < 0.001).

(J) Mean ΔF/F of the 470-nm signal (3-min bins) in AgRP neurons with II infusions of macronutrients in (G) (n = 6–8/group, two-way repeated-measures ANOVA, p < 0.001).

(K) Correlation between food intake and mean ΔF/F in AgRP neurons following intestinal infusion of macronutrients (n = 6–9/group, Pearson's correlation, p < 0.001).

Data are expressed as mean ± SEM; t tests and post hoc comparisons; ANOVA interaction, ∞∞∞p < 0.001; ANOVA main effect of group, ☼☼☼p < 0.001. See also Figures S1–S4.

on AgRP neuron activity, we performed bilateral subdiaphragmatic vagotomies (VGX) (Figure 2A). The success of these lesions was confirmed by the full attenuation of CCK effects on AgRP neuron activity (Figures 2B and 2C) (Alhadeff et al., 2019). VGX attenuated the effect of fat on AgRP neuron activity (Figures 2D and 2G). In contrast to fat, we noted that a complete diet of all macronutrients (Ensure) was still capable of reducing AgRP neuron activity in the absence of vagal signaling (Figures 2E and 2H), suggesting that macronutrients other than fat do not require the vagus to inhibit AgRP neuron activity. Strikingly, the effect of glucose was completely intact in mice following VGX (Figures 2F and 2I). These data demonstrate that vagal signaling is required for the effects of fat, but not glucose, on AgRP neuron activity.

Activation of the glucose sensor SGLT1 in the intestinal epithelium inhibits AgRP neuron activity

To determine how glucose is detected by AgRP neurons, we explored the molecular mediators that signal the presence of glucose in the intestine. Sodium-glucose linked transporters SGLT1 and SGLT3 sense glucose and SGLT1 transports glucose from the lumen of the intestine (Figure 3A) (Diez-Sampedro et al., 2003; Röder et al., 2014). Blockade of SGLT1/3 prevented the inhibition of AgRP neuron activity by glucose (Figures 3B–3E). Inhibition of GLUT2-dependent glucose transport does not significantly influence AgRP neuron activity (Figures 3B–3E). Interestingly, we find that activating SGLT1 is sufficient to mediate effects on AgRP neuron activity, as the non-metabolizable glucose analogs α-methyl-D-glucopyranoside (MDG, SGLT1/3 agonist) and 3-o-methylglucose (3-oMG, selective SGLT1 agonist) are each sufficient to inhibit AgRP neuron activity (Figures 3F–3H). Because increases in blood osmolarity reduce food intake (Gutman and Krausz, 1969), we explored the possibility that osmotic sensing contributes to glucose-induced AgRP neuron activity changes. While the osmotic content of low-concentration solutions (8%) does not influence AgRP neuron activity (i.e., equi-osmotic NaCl and mannitol have no effect; Figures 3F and 3I), highly osmotic solutions such as 16% mannitol, MDG, 3-oMG, glucose, and equi-osmotic concentrations of NaCl and urea all reduce AgRP neuron activity (Figures 3G–3I). However, the activity changes in response to the osmotic controls are smaller and delayed compared to SGLT1 agonists (Figure 3G). Thus, while intestinal osmosensors may contribute to glucose-mediated AgRP neuron activity reductions, the most robust effects on AgRP neuron activity are mediated by activation of SGLT1.

Spinal and hepatic portal signaling contribute to gut-AgRP glucose sensing

Because eliminating vagal signaling had no detectable impact on the ability of intestinal glucose to reduce AgRP neuron activity, we next sought to identify non-vagal pathways and post-absorptive mechanisms mediating the effects of glucose signaling. First, we explored the contribution of spinal afferents to glucose-mediated AgRP neuron activity reductions. We transected spinal (splanchnic) afferents innervating the abdominal viscera by performing a celiac-superior mesenteric ganglionectomy (CSMG; Figures 4A and 4B) (Bohland et al., 2014; Fujita and Donovan, 2005; Sclafani et al., 2003) in mice before moni-

toring AgRP neuron responses to intestinal glucose. Intestinal tissue extracted from mice with CSMG did not contain norepinephrine (Figure 4C) (Li et al., 2010), confirming successful nerve lesion. CSMG attenuated the effects of duodenal glucose (Figures 4D–4G) and eliminated the effects of ileal glucose on AgRP neuron activity (Figures 4H–4K). These findings highlight an underappreciated role for spinal afferents in mediating gut-hypothalamic signaling.

We next explored the role of post-absorptive glucose sensing in inhibiting AgRP neuron activity. Intraperitoneal (i.p.) injections of hypertonic glucose inhibited AgRP neuron activity (Figures 5A–5E), suggesting that blood glucose sensors may in fact mediate AgRP neuron activity changes. The hepatic portal vein (HPV) relays nutrients from the gut to the liver and is innervated by sensors that communicate with the brain in part via spinal afferent signaling (Baertschi and Vallet, 1981; Bohland et al., 2014; Choi-Kwon and Baertschi, 1991; Lechner et al., 2011). Furthermore, previous studies have implicated hepatic portal sensing in the gut-brain detection of glucose (Delaere et al., 2013; Mithieux et al., 2005; Zhang et al., 2018). Therefore, we directly examined the role of HPV sensing in gut-AgRP signaling by infusing glucose into the HPV while monitoring AgRP neuron activity in food-deprived mice (Figure 5F). We revealed a sustained reduction in AgRP neuron activity upon HPV infusion of glucose, but not fat (Figures 5G and 5H). Similar to duodenal sensing, this AgRP neuron activity reduction by HPV glucose also involves SGLT1, as HPV infusion of the selective SGLT1 agonist 3-oMG caused a robust suppression of neural activity (Figure 5K). This is not likely mediated by osmotic sensors, as equi-osmotic infusion of urea did not affect AgRP neuron activity (Figures 5G–5J). Interestingly, hypertonic solutions of sodium or potassium also trended toward a reduction in AgRP neuron activity, although the effects were not statistically significant compared to physiological saline (Figures 5L and 5M). These AgRP neuron activity dynamics observed during salt infusion are not entirely surprising given known cation sensors (e.g., NKCC1) expressed in the hepatoportal region (Tsuchiya et al., 2004). Taken together, these results suggest that HPV sensors are sufficient to inhibit AgRP neuron activity.

DISCUSSION

Here, we uncover post-ingestive mechanisms through which nutrients in the gut inhibit hunger neurons in the hypothalamus (Figure 5N). We demonstrate differences in how individual macronutrients are detected in the intestine and relayed to AgRP neurons. Regardless of the site of infusion or the nutrient infused, AgRP neuron activity responses to post-ingestive effects of nutrients are near-perfect indicators of feeding behavior. Taken together, these findings begin to reveal the complex labyrinth through which nutrients are relayed to hunger neurons, and the simplicity through which AgRP neurons integrate these signals to influence behavior.

Post-ingestive effects of food intake dominate changes in AgRP neuron activity (Beutler et al., 2017; Su et al., 2017), but the mechanisms mediating these effects are not fully known. Here we identify pathways and mechanisms through which nutrients communicate with AgRP neurons. First, fat in the duodenum engages vagal signaling to inhibit AgRP neurons. In
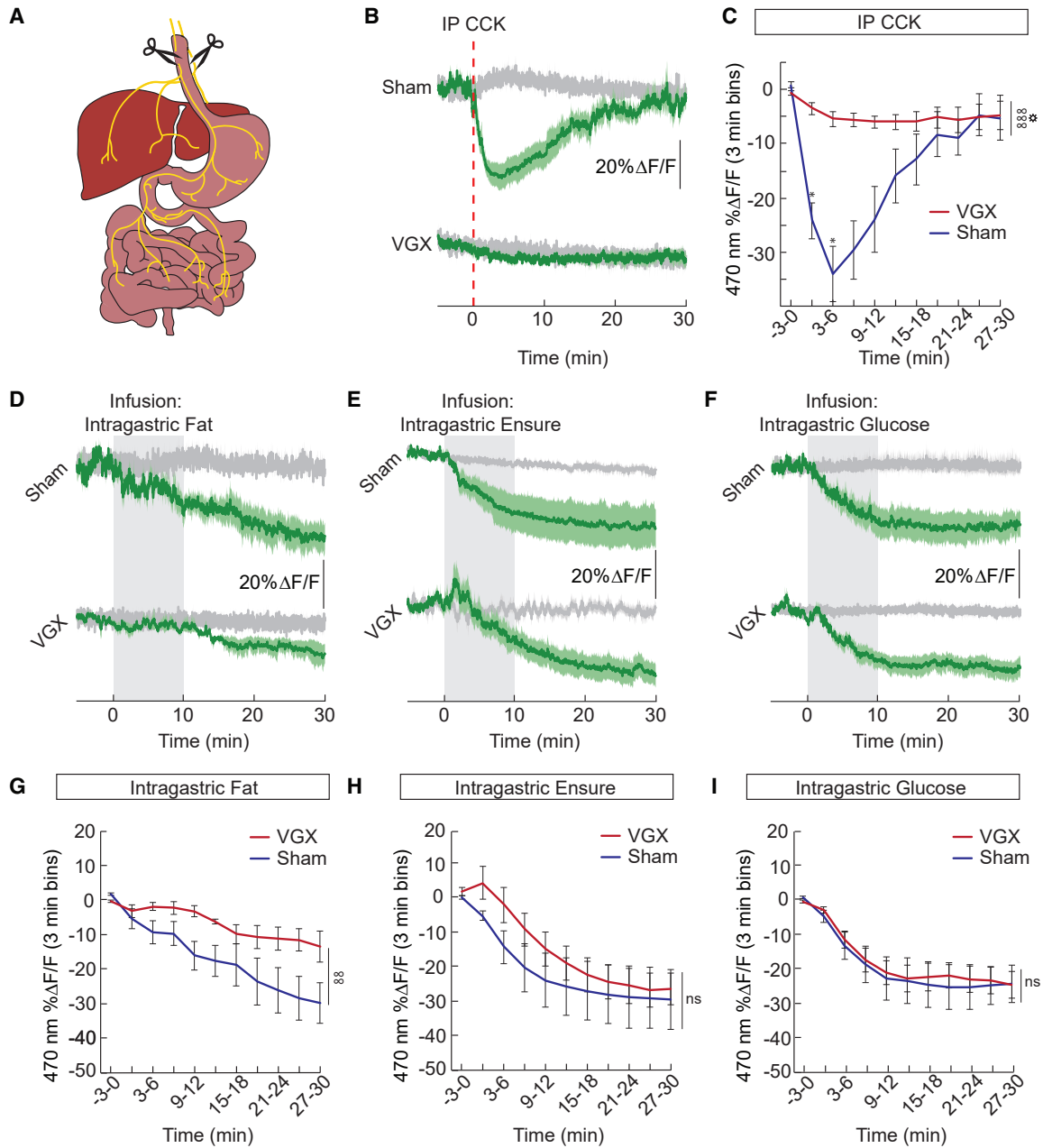
Cell Metabolism
Short Article

CellPress

Figure 2. Vagal-independent detection of glucose, but not fat, by hypothalamic neurons

(A) A complete subdiaphragmatic vagotomy (VGX) was performed to determine how vagal gut-brain signaling contributes to AgRP neuron activity in mice.

(B) Average ΔF/F of GCaMP6s signals in AgRP neurons of food-restricted VGX and sham mice following intraperitoneal (i.p.) injection of cholecystokinin (CCK, 30 μg/kg). Signals are aligned to the time of injection. Green, 470-nm calcium signal; gray, 405-nm control signal. Dark lines represent means and lighter shaded areas represent SEM.

(C) Mean ΔF/F of the 470-nm signal (3-min bins) of VGX and sham mice following i.p. injection of CCK (n = 5/group, two-way repeated-measures ANOVA, p < 0.001).

(D–F) Average ΔF/F of GCaMP6s signals in AgRP neurons of food-restricted VGX and sham mice with intra-gastric (IG) infusions of (D) fat (1 kcal), (E) Ensure (1 kcal), and (F) glucose (2/3 kcal). Signals are aligned to the start of infusion.

(G–I) Mean ΔF/F of the 470-nm signal (3-min bins) of VGX and sham mice following IG infusions of (G) fat (n = 4/group, two-way repeated-measures ANOVA, p < 0.01), (H) Ensure (n = 4–6/group, two-way repeated-measures ANOVA, ns), and (I) glucose (n = 6–7/group, two-way repeated-measures ANOVA, ns).

Data are expressed as mean ± SEM; ns, p > 0.05; t tests and post hoc comparisons, *p < 0.05; ANOVA interaction, ∞∞ p < 0.01, ∞∞∞ p < 0.001; ANOVA main effect of group, ☼p < 0.05.
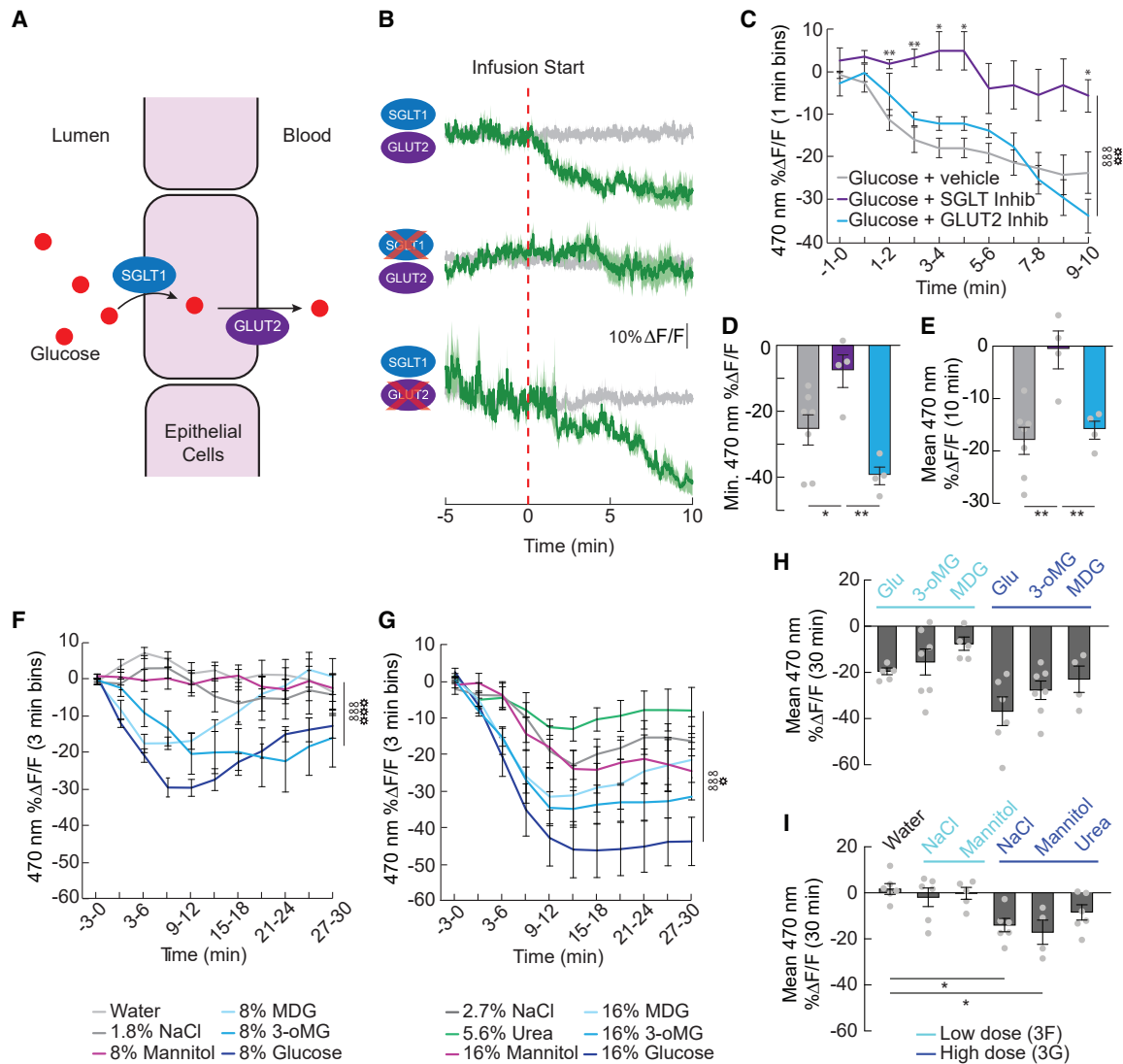
Figure 3. AgRP neurons detect SGLT1-mediated glucose uptake into the intestinal epithelium

(A) Glucose is transported into the intestinal epithelial cells by sodium-glucose linked transporter 1 (SGLT1) and out of the cells by glucose transporter 2 (GLUT2).

(B) Average ΔF/F of GCaMP6s signals in AgRP neurons of food-restricted mice during intra-duodenal (ID) infusions of 8% glucose (top), 8% glucose with the SGLT1/3 inhibitor phlorizin (0.4%, middle), and 8% glucose with the GLUT2 inhibitor phloretin (0.23%, bottom). Signals are aligned to the start of the infusion. Green, 470-nm control signal; gray, 405-nm control signal. Dark lines represent means and lighter shaded areas represent SEM.

(C) Mean ΔF/F of the 470-nm signal (1-min bins) in AgRP neurons during ID infusions of glucose solutions in (B) (n = 4–7/group, two-way repeated-measures ANOVA, p < 0.001).

(D) Minimum ΔF/F of the 470-nm signal during ID infusions of glucose solutions in (B) (n = 4–7/group, one-way ANOVA, p < 0.01).

(E) Mean ΔF/F of the 470-nm signal from 0 to 10 min during ID infusions of glucose solutions in (B) (n = 4–7/group, one-way ANOVA, p < 0.01).

(F) Mean ΔF/F of the 470-nm signal (3-min bins) in AgRP neurons with ID infusions of water; 8% glucose, mannitol, methyl α-D-glucopyranoside (MDG), 3-o-methylglucose (3-oMG), or glucose; or equi-osmotic (1.8%) NaCl (n = 5–7/group, two-way repeated-measures ANOVA, p < 0.001). Signals were aligned to the start of the infusion.

(G) Mean ΔF/F of the 470-nm signal (3-min bins) in AgRP neurons with ID infusions of 16% mannitol, MDG, 3-oMG, glucose, NaCl (2.7%), or urea (5.6%) (n = 4–7/group, two-way repeated-measures ANOVA, p < 0.001).

(H) Mean ΔF/F of the 470-nm signal from 0 to 30 min following duodenal infusion of glucose and SGLT agonists. Low concentrations from (F) are in light blue and high concentrations from (G) are in dark blue (n = 4–7/group, one-way repeated ANOVA, p < 0.01).

(I) Mean ΔF/F of the 470-nm signal from 0 to 30 min following duodenal infusion of non-nutritive NaCl, mannitol, and urea. Low concentrations from (F) are in light blue and high concentrations from (G) are in dark blue (n = 4–6/group, one-way repeated ANOVA, p < 0.01).

Data are expressed as mean ± SEM; ns, p > 0.05; t tests and post hoc comparisons, *p < 0.05, **p < 0.01; ANOVA interaction, ∞ ∞ ∞ p < 0.001; ANOVA main effect of group, ☼p < 0.05, ☼☼p < 0.01, ☼☼☼p < 0.001.
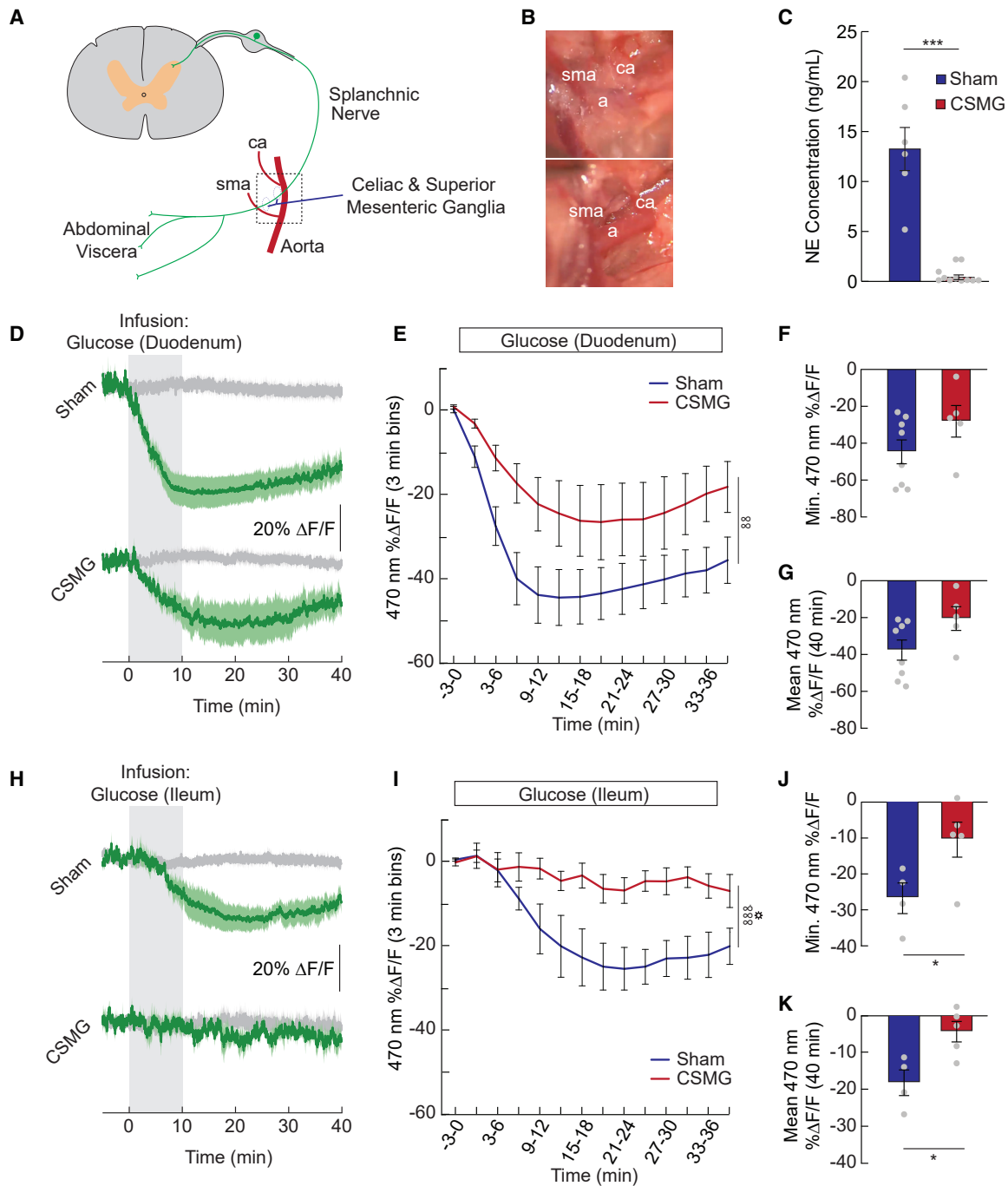
Figure 4. AgRP neuron inhibition by intestinal glucose is signaled in part by spinal afferents

(A) Schematic depicting a splanchnic afferent neuron innervating the gut and passing through the celiac and superior mesenteric ganglia.

(B) Images showing the area depicted by the dotted square in (A). The aorta (a), celiac artery (ca), and superior mesenteric artery (sma) were isolated (top) and cleared of all lymphatic and nervous tissue (bottom) to ablate spinal afferent signaling from the gut.

(C) Norepinephrine (NE) concentration in the supernatant from homogenized intestinal tissue of sham and CSMG mice (n = 6–11/group, unpaired t test, p < 0.001).

(D) Average ΔF/F of GCaMP6s signals in AgRP neurons of food-restricted sham and CSMG mice during infusions of glucose (2/3 kcal) in the duodenum. Signals are aligned to the start of infusion. Green, 470-nm calcium signal; gray, 405-nm control signal. Dark lines represent means and lighter shaded areas represent SEM.

(E) Mean ΔF/F of the 470-nm signal (3-min bins) of sham and CSMG mice during infusions of glucose in the duodenum (n = 5–8/group, two-way repeated-measures ANOVA, p < 0.01).

(F) Minimum ΔF/F of the 470-nm signal in sham and CSMG mice during infusions of glucose in the duodenum (n = 5–8/group, unpaired t test, ns).

(G) Mean ΔF/F of the 470-nm signal from 0 to 40 min during infusions of glucose in the duodenum (n = 5–8/group, unpaired t test, p = 0.07).

contrast, SGLT1-dependent glucose uptake into the intestinal epithelium inhibits AgRP neuron activity and utilizes spinal afferent signaling. After nutrient absorption, hepatic portal detection of glucose provides a redundant mechanism to inhibit AgRP neuron activity. The HPV is exposed to the largest range of post-absorptive glucose concentrations compared to the rest of the body, so it is well suited to mediate gut-brain glucose signaling (Soty et al., 2017). Our studies complement other findings that SGLT1/3 is required for HPV glucose-mediated food intake reductions (Delaere et al., 2012).

We demonstrated that fat absorbed in the duodenum requires vagal signaling to influence AgRP neuron activity. Interestingly, while both triglyceride and fatty acid infused in the duodenum inhibit food intake and AgRP neuron activity, ileal fatty acid also inhibits food intake, but *not* AgRP neuron activity. Why is there no effect on AgRP neuron activity? One possibility is that the food intake reduction occurs due to ileal fat initiating the "ileal brake," a mechanism that likely inhibits food intake by slowing gut motility and maintaining gastric distension (Brown et al., 1990; Pironi et al., 1993; Welch et al., 1988). AgRP neuron activity is therefore not influenced because gastric distension alone does not affect AgRP neuron activity (Beutler et al., 2017; Su et al., 2017). It has recently been suggested that intestinal distension is the main source of vagal input that ultimately influences AgRP neuron activity (Bai et al., 2019). However, while activity in vagal intestinal mechanoreceptor-expressing neurons is sufficient to reduce AgRP neuron activity (Bai et al., 2019), our findings demonstrate that intestinal stretch is not necessary because (1) the full effects of glucose are preserved in the absence of vagal signaling and (2) bypassing the intestines with direct HPV infusions is sufficient to inhibit AgRP neuron activity.

Our data add to the literature on the pathways that transmit sugar signals to the brain by highlighting the effects of spinal afferent signaling on AgRP neuron activity. Glucose in the duodenum also activates vagal afferents (Schwartz and Moran, 1998; Tan et al., 2020; Williams et al., 2016), although our data demonstrate that vagal transmission is not *required* for the effects of glucose on AgRP neuron activity. However, CSMG only partially attenuated the effects of duodenal glucose on AgRP neuron activity, suggesting that other pathways (vagal, humoral) may contribute to these glucose-mediated neural activity changes. Interestingly, CSMG abolished the effects of ileal glucose on AgRP neuron activity, suggesting that spinal afferents control the inhibition of AgRP neuron activity by ileal, and likely hepatic portal, glucose. Our data add to a growing body of literature suggesting that spinal afferents mediate portal glucose signaling (Delaere et al., 2012; Soty et al., 2017). Overall, our findings reveal multiple pathways through which nutrient signals are relayed to hypothalamic circuits in the brain.

Our finding that vagal signaling is not required for glucose-mediated AgRP neuron inhibition is interesting in light of the controversial role of the vagus nerve in mediating post-oral sugar preference. It has been demonstrated that preferences develop to flavors paired with intestinal infusion of glucose, and these preferences do not require vagal signaling (Lucas and Sclafani, 1996; Qu et al., 2019; Sclafani et al., 2003; Sclafani and Lucas, 1996). In contrast, recent findings highlight vagal gut-brain signaling in transmitting sugar preferences and influencing dopamine signaling (Fernandes et al., 2020; Tan et al., 2020). Across studies, however, there is agreement that SGLT1-mediated glucose transport is necessary for the formation of sugar preferences (Sclafani et al., 2016; Tan et al., 2020; Zukerman et al., 2013). Our data support a non-vagal, SGLT1-dependent spinal mechanism through which glucose reduces activity in AgRP neurons. It will be important for future studies to reveal whether AgRP neuron activity contributes to the formation of nutrient preferences, especially because inhibition of AgRP neuron activity in hungry mice conditions flavor and place preferences (Betley et al., 2015). Furthermore, since spinal afferents in part mediate the effect of glucose on AgRP neuron activity, the role of redundant pathways for gut-brain glucose signaling should be investigated in the context of sugar reinforcement.

The duodenum is the primary site of nutrient absorption (Breen et al., 2013), so it follows that the inhibition of AgRP neurons is greater in response to duodenal- versus ileal-infused nutrients. However, the ability of ileal or hepatic portal sugar to be detected at the level of AgRP neurons could have important implications for disease conditions, such as inflammatory bowel or celiac disease, involving nutrient malabsorption. Furthermore, ileal detection and absorption of nutrients becomes physiologically relevant for patients undergoing Roux-en-Y surgery for weight loss, as nutrients bypass most or all of the proximal small intestine depending on the surgical technique used (Abdeen and le Roux, 2016). In these cases, a post-duodenal mechanism for the detection and absorption of nutrients becomes especially important.

While feeding behavior is influenced by distributed neural circuits (Andermann and Lowell, 2017), our data suggest that changes in AgRP neuron activity in response to gastrointestinal nutrients are a remarkable predictor of feeding behavior. Indeed, we uncover a strong correlation between food intake and AgRP neuron inhibition resulting from duodenal and ileal infusion of nutrients. There are, however, examples of substances that inhibit AgRP neuron activity and not food intake, or vice versa. For example, some drugs of abuse (e.g., alcohol) inhibit AgRP neuron activity without influencing food intake (Alhadeff et al., 2019). Conversely, incretin hormones (e.g., GLP-1) and noxious agents (e.g., lithium chloride or lipopolysaccharide) inhibit food intake but do not affect AgRP neuron activity (Beutler et al., 2017; Su et al., 2017). However, these perturbations cause

(H) Average ΔF/F of GCaMP6s signals in AgRP neurons of food-restricted sham and CSMG mice during infusions of glucose (2/3 kcal) in the ileum.

(I) Mean ΔF/F of the 470-nm signal (3-min bins) of sham and CSMG mice during infusions of glucose in the ileum (n = 4–5/group, two-way repeated-measures ANOVA, p < 0.001).

(J) Minimum ΔF/F of the 470-nm signal in sham and CSMG mice during infusions of glucose in the ileum (n = 4–5/group, unpaired t test, p < 0.05).

(K) Mean ΔF/F of the 470-nm signal from 0 to 40 min during infusions of glucose in the ileum (n = 4–5/group, unpaired t test, p < 0.05).

Data are expressed as mean ± SEM; ns, p > 0.05; *p < 0.05, ***p < 0.001; ANOVA interaction, ∞∞p < 0.01, ∞∞∞p < 0.001; ANOVA main effect of group, ☼p < 0.05.
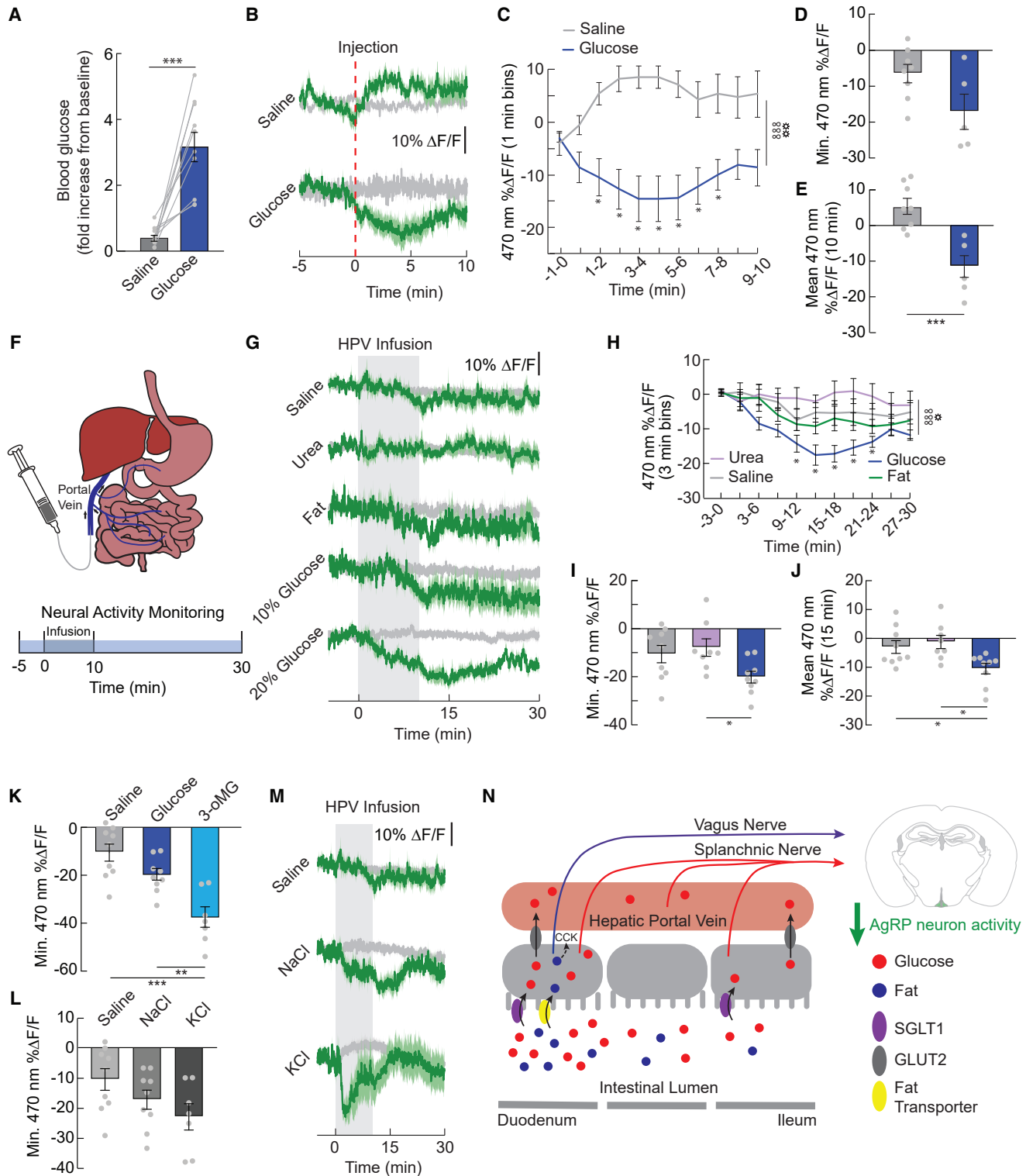
Figure 5. AgRP neurons detect glucose in the hepatic portal vein

(A) Increase in blood glucose levels 10 min post-injection of i.p. glucose (2 g/kg) or equi-osmotic NaCl (n = 10/group, paired t test, p < 0.001).

(B) Average ΔF/F of GCaMP6s signals in AgRP neurons of food-restricted mice following i.p. injection of saline or glucose. Signals are aligned to the start of the infusion. Green, 470-nm calcium signal; gray, 405-nm control signal. Dark lines represent means and lighter shaded areas represent SEM.

(C) Mean ΔF/F of the 470-nm signal (1-min bins) in AgRP neurons during i.p. injections of saline or glucose (n = 5–8/group, two-way repeated-measures ANOVA, p < 0.001).

anorexia that is mediated at least in part by activating sickness pathways, rather than inhibiting hunger circuits. This may in part explain why ileal fatty acid inhibits food intake but not AgRP neuron activity. Thus, while there are many pathways to inhibit food intake, our data suggest that AgRP neuron activity reflects availability of utilizable calories in the gut.

Conclusion

For a behavior as fundamental as food intake, it is appreciated that there are redundant circuits to ensure sufficient feeding behavior. It is equally important for food intake to be tightly regulated and for feeding to cease when nutrients are acquired. We uncovered multiple mechanisms for the *in vivo* inhibition of hunger circuits in the brain, adding another dimension to the plexus of food intake regulation.

Limitations of study

The experiments in this study rely on the use of calcium dynamics as a proxy for neural activity. A limitation of this technique is that we cannot directly correlate increases in calcium activity with action potentials. That being said, the relationship between *ex vivo* GCaMP fluorescence and cell spiking is characterized (Betley et al., 2015), and calcium dynamics are therefore commonly used as an indicator of AgRP neuron activity. Another limitation of our study involves the use of neural lesions to evaluate the contributions of gut-brain nutrient signaling on AgRP neuron activity. While these blunt lesions provide valuable information on the necessity of vagal and spinal signaling, it will be important for future studies to determine the specific neurons and signaling pathways that transmit nutritive signals to the brain following intestinal detection of fat or sugar. Finally, we note that our splanchnic lesion (CSMG) damages efferent fibers including some vagal efferents (Berthoud and Powley, 1993), potentially constraining the interpretation of these data. However, it is unlikely that efferent signaling contributes to gut-hypothalamic signaling, and subdiaphragmatic vagotomy had no effect on glucose-mediated AgRP neuron inhibition. Therefore, we believe that the ability of CSMG to eliminate these effects is due to spinal afferent signaling.

STAR★METHODS

Detailed methods are provided in the online version of this paper and include the following:

SUPPLEMENTAL INFORMATION

Supplemental Information can be found online at https://doi.org/10.1016/j.cmet.2020.12.018.

AUTHOR CONTRIBUTIONS

N.G., J.N.B., and A.L.A. initiated the project and prepared the manuscript with comments from all authors. N.G., A.D.M., J.R.E.C., M.A., J.N.B., and A.L.A. designed experiments, performed experiments, and/or analyzed data.

(D) Minimum $\Delta F/F$ of the 470-nm signal during i.p. injections of solutions in (J) ($n = 5–8$/group, unpaired t test, $p = 0.06$).

(E) Mean $\Delta F/F$ of the 470-nm signal from 0 to 10 min during i.p. injections of solutions in (J) ($n = 5–8$/group, unpaired t test, $p < 0.001$).

(F) Nutrients were infused into the hepatic portal vein (HPV) and AgRP neuron activity was monitored.

(G) Average $\Delta F/F$ of GCaMP6s signals in AgRP neurons of food-restricted mice during HPV infusions of saline, urea (6.7%), fat (8% Intralipid, 0.4 kcal), 10% glucose (0.2 kcal), and 20% glucose (0.4 kcal).

(H) Mean $\Delta F/F$ of the 470-nm signal (3-min bins) in AgRP neurons with HPV infusions of saline, urea, fat, or 20% glucose ($n = 8–9$/group, two-way repeated-measures ANOVA, $p < 0.001$).

(I) Minimum $\Delta F/F$ of the 470-nm signal following HPV infusions of saline, urea, or 20% glucose ($n = 8–9$/group, one-way ANOVA, $p < 0.05$).

(J) Mean $\Delta F/F$ of the 470-nm signal from 0 to 15 min following infusions of saline, urea, or 20% glucose ($n = 8–9$/group, one-way ANOVA, $p < 0.05$).

(K) Minimum $\Delta F/F$ of the 470-nm signal following HPV infusions of saline, glucose, or 3-oMG ($n = 7–9$/group, one-way ANOVA, $p < 0.001$).

(L) Minimum $\Delta F/F$ of the 470-nm signal following HPV infusions of saline, 3.6% NaCl, or 2.2% KCl ($n = 7–9$/group, one-way ANOVA, $p = 0.09$).

(M) Average $\Delta F/F$ of GCaMP6s signals during HPV infusions of saline, NaCl (3.6%), or KCl (2.2%).

(N) Model depicting our findings on the gut-brain signaling pathways necessary for the inhibition of AgRP neurons by fat and glucose.

Data are expressed as mean ± SEM; ns, $p > 0.05$; t tests and post hoc comparisons, *$p < 0.05$, **$p < 0.01$, ***$p < 0.001$; ANOVA interaction, $\infty\infty\infty$ $p < 0.001$; ANOVA main effect of group, ☼$p < 0.05$, ☼☼$p < 0.01$.

Cell Metabolism
Short Article

CellPress

REFERENCES

Abdeen, G., and le Roux, C.W. (2016). Mechanism underlying the weight loss and complications of Roux-en-Y gastric bypass. Review. Obes. Surg. 26, 410–421.

Alhadeff, A.L., Su, Z., Hernandez, E., Klima, M.L., Phillips, S.Z., Holland, R.A., Guo, C., Hantman, A.W., De Jonghe, B.C., and Betley, J.N. (2018). A neural circuit for the suppression of pain by a competing need state. Cell 173, 140–152.e15.

Alhadeff, A.L., Goldstein, N., Park, O., Klima, M.L., Vargas, A., and Betley, J.N. (2019). Natural and drug rewards engage distinct pathways that converge on coordinated hypothalamic and reward circuits. Neuron 103, 891–908.e6.

Andermann, M.L., and Lowell, B.B. (2017). Toward a wiring diagram understanding of appetite control. Neuron 95, 757–778.

Aponte, Y., Atasoy, D., and Sternson, S.M. (2011). AGRP neurons are sufficient to orchestrate feeding behavior rapidly and without training. Nat. Neurosci. 14, 351–355.

Baertschi, A.J., and Vallet, P.G. (1981). Osmosensitivity of the hepatic portal vein area and vasopressin release in rats. J. Physiol. 315, 217–230.

Bai, L., Mesgarzadeh, S., Ramesh, K.S., Huey, E.L., Liu, Y., Gray, L.A., Aitken, T.J., Chen, Y., Beutler, L.R., Ahn, J.S., et al. (2019). Genetic identification of vagal sensory neurons that control feeding. Cell 179, 1129–1143.e23.

Batterham, R.L., Cowley, M.A., Small, C.J., Herzog, H., Cohen, M.A., Dakin, C.L., Wren, A.M., Brynes, A.E., Low, M.J., Ghatei, M.A., et al. (2002). Gut hormone PYY(3-36) physiologically inhibits food intake. Nature 418, 650–654.

Bell, S.J., Bradley, D., Forse, R.A., and Bistrian, B.R. (1997). The new dietary fats in health and disease. J. Am. Diet. Assoc. 97, 280–286, quiz 287–288.

Berthoud, H.R., and Powley, T.L. (1993). Characterization of vagal innervation to the rat celiac, suprarenal and mesenteric ganglia. J. Auton. Nerv. Syst. 42, 153–169.

Berthoud, H.R., Blackshaw, L.A., Brookes, S.J., and Grundy, D. (2004). Neuroanatomy of extrinsic afferents supplying the gastrointestinal tract. Neurogastroenterol. Motil. 16 (Suppl 1), 28–33.

Betley, J.N., Xu, S., Cao, Z.F.H., Gong, R., Magnus, C.J., Yu, Y., and Sternson, S.M. (2015). Neurons for hunger and thirst transmit a negative-valence teaching signal. Nature 521, 180–185.

Beutler, L.R., Chen, Y., Ahn, J.S., Lin, Y.C., Essner, R.A., and Knight, Z.A. (2017). Dynamics of gut-brain communication underlying hunger. Neuron 96, 461–475.e5.

Bohland, M., Matveyenko, A.V., Saberi, M., Khan, A.M., Watts, A.G., and Donovan, C.M. (2014). Activation of hindbrain neurons is mediated by portal-mesenteric vein glucosensors during slow-onset hypoglycemia. Diabetes 63, 2866–2875.

Breen, D.M., Rasmussen, B.A., Côté, C.D., Jackson, V.M., and Lam, T.K. (2013). Nutrient-sensing mechanisms in the gut as therapeutic targets for diabetes. Diabetes 62, 3005–3013.

Brookes, S.J., Spencer, N.J., Costa, M., and Zagorodnyuk, V.P. (2013). Extrinsic primary afferent signalling in the gut. Nat. Rev. Gastroenterol. Hepatol. 10, 286–296.

Brown, N.J., Read, N.W., Richardson, A., Rumsey, R.D., and Bogentoft, C. (1990). Characteristics of lipid substances activating the ileal brake in the rat. Gut 31, 1126–1129.

Castelli, W.P. (1986). The triglyceride issue: a view from Framingham. Am. Heart J. 112, 432–437.

Chambers, A.P., Sandoval, D.A., and Seeley, R.J. (2013). Integration of satiety signals by the central nervous system. Curr. Biol. 23, R379–R388.

Chen, Y., Lin, Y.C., Kuo, T.W., and Knight, Z.A. (2015). Sensory detection of food rapidly modulates arcuate feeding circuits. Cell 160, 829–841.

Choi-Kwon, S., and Baertschi, A.J. (1991). Splanchnic osmosensation and vasopressin: mechanisms and neural pathways. Am. J. Physiol. 261, E18–E25.

de Araujo, I.E., Schatzker, M., and Small, D.M. (2020). Rethinking food reward. Annu. Rev. Psychol. 71, 139–164.

Delaere, F., Duchampt, A., Mounien, L., Seyer, P., Duraffourd, C., Zitoun, C., Thorens, B., and Mithieux, G. (2012). The role of sodium-coupled glucose co-transporter 3 in the satiety effect of portal glucose sensing. Mol. Metab. 2, 47–53.

Delaere, F., Akaoka, H., De Vadder, F., Duchampt, A., and Mithieux, G. (2013). Portal glucose influences the sensory, cortical and reward systems in rats. Eur. J. Neurosci. 38, 3476–3486.

Dezfuli, G., Gillis, R.A., Tatge, J.E., Duncan, K.R., Dretchen, K.L., Jackson, P.G., Verbalis, J.G., and Sahibzada, N. (2018). Subdiaphragmatic vagotomy with pyloroplasty ameliorates the obesity caused by genetic deletion of the melanocortin 4 receptor in the mouse. Front. Neurosci. 12, 104.

Diez-Sampedro, A., Hirayama, B.A., Osswald, C., Gorboulev, V., Baumgarten, K., Volk, C., Wright, E.M., and Koepsell, H. (2003). A glucose sensor hiding in a family of transporters. Proc. Natl. Acad. Sci. USA 100, 11753–11758.

Fernandes, A.B., Alves da Silva, J., Almeida, J., Cui, G., Gerfen, C.R., Costa, R.M., and Oliveira-Maia, A.J. (2020). Postingestive modulation of food seeking depends on vagus-mediated dopamine neuron activity. Neuron 106, 778–788.e6.

Fox, E.A., Phillips, R.J., Martinson, F.A., Baronowsky, E.A., and Powley, T.L. (2000). Vagal afferent innervation of smooth muscle in the stomach and duodenum of the mouse: morphology and topography. J. Comp. Neurol. 428, 558–576.

Fujita, S., and Donovan, C.M. (2005). Celiac-superior mesenteric ganglionectomy, but not vagotomy, suppresses the sympathoadrenal response to insulin-induced hypoglycemia. Diabetes 54, 3258–3264.

Gutman, Y., and Krausz, M. (1969). Regulation of food and water intake in rats as related to plasma osmolarity and volume. Physiol. Behav. 4, 311–313.

Han, W., Tellez, L.A., Niu, J., Medina, S., Ferreira, T.L., Zhang, X., Su, J., Tong, J., Schwartz, G.J., van den Pol, A., and de Araujo, I.E. (2016). Striatal dopamine links gastrointestinal rerouting to altered sweet appetite. Cell Metab. 23, 103–112.

Johnstone, L.E., Fong, T.M., and Leng, G. (2006). Neuronal activation in the hypothalamus and brainstem during feeding in rats. Cell Metab. 4, 313–321.

Krashes, M.J., Koda, S., Ye, C., Rogan, S.C., Adams, A.C., Cusher, D.S., Maratos-Flier, E., Roth, B.L., and Lowell, B.B. (2011). Rapid, reversible activation of AgRP neurons drives feeding behavior in mice. J. Clin. Invest. 121, 1424–1428.

Lechner, S.G., Markworth, S., Poole, K., Smith, E.S., Lapatsina, L., Frahm, S., May, M., Pischke, S., Suzuki, M., Ibañez-Tallon, I., et al. (2011). The molecular and cellular identity of peripheral osmoreceptors. Neuron 69, 332–344.

Lerner, T.N., Shilyansky, C., Davidson, T.J., Evans, K.E., Beier, K.T., Zalocusky, K.A., Crow, A.K., Malenka, R.C., Luo, L., Tomer, R., and Deisseroth, K. (2015). Intact-brain analyses reveal distinct information carried by SNc dopamine subcircuits. Cell 162, 635–647.

Levin, B.E., Dunn-Meynell, A.A., and Routh, V.H. (1999). Brain glucose sensing and body energy homeostasis: role in obesity and diabetes. Am. J. Physiol. 276, R1223–R1231.

Li, Z., Caron, M.G., Blakely, R.D., Margolis, K.G., and Gershon, M.D. (2010). Dependence of serotonergic and other nonadrenergic enteric neurons on norepinephrine transporter expression. J. Neurosci. 30, 16730–16740.

Lucas, F., and Sclafani, A. (1996). Capsaicin attenuates feeding suppression but not reinforcement by intestinal nutrients. Am. J. Physiol. 270, R1059–R1064.

Lutz, T.A. (2006). Amylinergic control of food intake. Physiol. Behav. 89, 465–471.

Mandelblat-Cerf, Y., Ramesh, R.N., Burgess, C.R., Patella, P., Yang, Z., Lowell, B.B., and Andermann, M.L. (2015). Arcuate hypothalamic AgRP and putative POMC neurons show opposite changes in spiking across multiple timescales. eLife 4, e07122.

Mithieux, G., Misery, P., Magnan, C., Pillot, B., Gautier-Stein, A., Bernard, C., Rajas, F., and Zitoun, C. (2005). Portal sensing of intestinal gluconeogenesis is a mechanistic link in the diminution of food intake induced by diet protein. Cell Metab. 2, 321–329.

Moran, T.H., Ladenheim, E.E., and Schwartz, G.J. (2001). Within-meal gut feedback signaling. Int. J. Obes. Relat. Metab. Disord. 25 (Suppl 5), S39–S41.

Olson, B.R., Freilino, M., Hoffman, G.E., Stricker, E.M., Sved, A.F., and Verbalis, J.G. (1993). c-Fos expression in rat brain and brainstem nuclei in response to treatments that alter food intake and gastric motility. Mol. Cell. Neurosci. 4, 93–106.

Phifer, C.B., and Berthoud, H.R. (1998). Duodenal nutrient infusions differentially affect sham feeding and Fos expression in rat brain stem. Am. J. Physiol. 274, R1725–R1733.

Pironi, L., Stanghellini, V., Miglioli, M., Corinaldesi, R., De Giorgio, R., Ruggeri, E., Tosetti, C., Poggioli, G., Morselli Labate, A.M., Monetti, N., et al. (1993). Fat-induced ileal brake in humans: a dose-dependent phenomenon correlated to the plasma levels of peptide YY. Gastroenterology 105, 733–739.

Qu, T., Han, W., Niu, J., Tong, J., and de Araujo, I.E. (2019). On the roles of the duodenum and the vagus nerve in learned nutrient preferences. Appetite 139, 145–151.

Riera, C.E., Tsaousidou, E., Halloran, J., Follett, P., Hahn, O., Pereira, M.M.A., Ruud, L.E., Alber, J., Tharp, K., Anderson, C.M., et al. (2017). The sense of smell impacts metabolic health and obesity. Cell Metab. 26, 198–211.e5.

Röder, P.V., Geillinger, K.E., Zietek, T.S., Thorens, B., Koepsell, H., and Daniel, H. (2014). The role of SGLT1 and GLUT2 in intestinal glucose transport and sensing. PLoS One 9, e89977.

Schwartz, G.J., and Moran, T.H. (1998). Duodenal nutrient exposure elicits nutrient-specific gut motility and vagal afferent signals in rat. Am. J. Physiol. 274, R1236–R1242.

Sclafani, A., and Ackroff, K. (2018). Role of lipolysis in postoral and oral fat preferences in mice. Am. J. Physiol. Regul. Integr. Comp. Physiol. 315, R434–R441.

Sclafani, A., and Lucas, F. (1996). Abdominal vagotomy does not block carbohydrate-conditioned flavor preferences in rats. Physiol. Behav. 60, 447–453.

Sclafani, A., Ackroff, K., and Schwartz, G.J. (2003). Selective effects of vagal deafferentation and celiac-superior mesenteric ganglionectomy on the reinforcing and satiating action of intestinal nutrients. Physiol. Behav. 78, 285–294.

Sclafani, A., Koepsell, H., and Ackroff, K. (2016). SGLT1 sugar transporter/sensor is required for post-oral glucose appetition. Am. J. Physiol. Regul. Integr. Comp. Physiol. 310, R631–R639.

Soty, M., Gautier-Stein, A., Rajas, F., and Mithieux, G. (2017). Gut-brain glucose signaling in energy homeostasis. Cell Metab. 25, 1231–1242.

Su, Z., Alhadeff, A.L., and Betley, J.N. (2017). Nutritive, post-ingestive signals are the primary regulators of AgRP neuron activity. Cell Rep. 21, 2724–2736.

Takahashi, K.A., and Cone, R.D. (2005). Fasting induces a large, leptin-dependent increase in the intrinsic action potential frequency of orexigenic arcuate nucleus neuropeptide Y/Agouti-related protein neurons. Endocrinology 146, 1043–1047.

Tan, H.E., Sisti, A.C., Jin, H., Vignovich, M., Villavicencio, M., Tsang, K.S., Goffer, Y., and Zuker, C.S. (2020). The gut-brain axis mediates sugar preference. Nature 580, 511–516.

Tong, Q., Ye, C.P., Jones, J.E., Elmquist, J.K., and Lowell, B.B. (2008). Synaptic release of GABA by AgRP neurons is required for normal regulation of energy balance. Nat. Neurosci. 11, 998–1000.

Tordoff, M.G., and Friedman, M.I. (1986). Hepatic portal glucose infusions decrease food intake and increase food preference. Am. J. Physiol. 251, R192–R196.

Tordoff, M.G., Tluczek, J.P., and Friedman, M.I. (1989). Effect of hepatic portal glucose concentration on food intake and metabolism. Am. J. Physiol. 257, R1474–R1480.

Tsuchiya, Y., Nakashima, S., Banno, Y., Suzuki, Y., and Morita, H. (2004). Effect of high-NaCl or high-KCl diet on hepatic Na+- and K+-receptor sensitivity and NKCC1 expression in rats. Am. J. Physiol. Regul. Integr. Comp. Physiol. 286, R591–R596.

Tsurugizawa, T., Kondoh, T., and Torii, K. (2008). Forebrain activation induced by postoral nutritive substances in rats. Neuroreport 19, 1111–1115.

Welch, I.M., Cunningham, K.M., and Read, N.W. (1988). Regulation of gastric emptying by ileal nutrients in humans. Gastroenterology 94, 401–404.

Williams, E.K., Chang, R.B., Strochlic, D.E., Umans, B.D., Lowell, B.B., and Liberles, S.D. (2016). Sensory neurons that detect stretch and nutrients in the digestive system. Cell 166, 209–221.

Woltman, T., and Reidelberger, R. (1995). Effects of duodenal and distal ileal infusions of glucose and oleic acid on meal patterns in rats. Am. J. Physiol. 269, R7–R14.

Yox, D.P., Stokesberry, H., and Ritter, R.C. (1991). Fourth ventricular capsaicin attenuates suppression of sham feeding induced by intestinal nutrients. Am. J. Physiol. 260, R681–R687.

Zalocusky, K.A., Ramakrishnan, C., Lerner, T.N., Davidson, T.J., Knutson, B., and Deisseroth, K. (2016). Nucleus accumbens D2R cells signal prior outcomes and control risky decision-making. Nature 531, 642–646.

Zhang, L., Han, W., Lin, C., Li, F., and de Araujo, I.E. (2018). Sugar metabolism regulates flavor preferences and portal glucose sensing. Front. Integr. Nuerosci. 12, 57.

Zukerman, S., Ackroff, K., and Sclafani, A. (2013). Post-oral appetite stimulation by sugars and nonmetabolizable sugar analogs. Am. J. Physiol. Regul. Integr. Comp. Physiol. 305, R840–R853.

Cell Metabolism
Short Article

STAR★METHODS

KEY RESOURCES TABLE

REAGENT or RESOURCE	SOURCE	IDENTIFIER
Bacterial and Viral Strains		
AAV1.Syn.Flex.GcaMP6s.WPRE.SV40	Addgene	100845
Chemicals, Peptides, and Recombinant Proteins		
Dulbecco's phosphate-buffered saline	HyClone	SH30013.04
Paraformaldehyde	MP Biomedicals	150146
Isoflurane	Clipper	0010250
Meloxicam	Norbrook Laboratories	55529-040-11
Bupivacaine	Moore Medical	52683
Hydrogen peroxide	Ricca Chemical Company	R3821310-1BV
Sodium chloride (NaCl)	Sigma-Aldrich	S7653-250G
Sterile saline	Pfizer	00409-4888-12
Intralipid	Fresenius Kabi	NDC 0338-0519-13
D-glucose	Sigma-Aldrich	G8270-100G
Ensure Plus, Vanilla	Abbott	53642
Proteinex- 18 Liquid solution	Llorens Pharmaceutical	54859-535-30
Cholecystokinin Octapeptide	Bachem	4033010
Methyl α-D-glucopyranoside	Sigma-Aldrich	M9376
D-Mannitol	Sigma-Aldrich	M4125
Phlorizin	Tocris	4627
Phloretin	Sigma-Aldrich	P7912
Orlistat	Sigma-Aldrich	O4139
Oleic Acid	VWR	112-80-1
Trisodium citrate dihydrate	Sigma-Aldrich	S1804
Heparin sodium	Midwest Vet	191.46750.3
Glycerol	Sigma-Aldrich	G7893
Urea	Sigma-Aldrich	PHR1406
Potassium Chloride	EMD Millipore	529552
3-O-Methyl-D-glucopyranose	Sigma-Aldrich	M4879
Cyanoacrylate glue	Loctite	4061
Premilene Mesh	B. Braun	1064435
Experimental Models: Organisms/Strains		
Mouse:AgRP-IRES-Cre Agrp$^{tm1(cre)Lowl}$/J	The Jackson Laboratory	012899
Mouse: C57BL/6J	The Jackson Laboratory	000664
Software and Algorithms		
MATLAB R2016a	MathWorks	https://www.mathworks.com/products/matlab.html
Synapse	Tucker-Davis Technologies	http://www.tdt.com/Synapse/index.html
Prism 8	GraphPad	https://www.graphpad.com/scientific-software/prism/
Other		
Microliter syringe pump, PHD Ultra	Harvard Apparatus	703007
Optic fibers for fiber photometry	Doric	MF2.5, 400/430-0.48
405 nm LED	ThorLabs	M405F1
490 nm LED	ThorLabs	M470F3
Amplifier	Tucker-Davis Technology	RZ5P

(*Continued on next page*)

Continued

REAGENT or RESOURCE	SOURCE	IDENTIFIER
Femtowatt photoreceiver	Newport	2151
Metabond	Parkell	S380
Ortho-jet BCA Liquid	Lang Dental Manufacturing	B1306
Jet Tooth Shade Powder	Lang Dental Manufacturing	143069
Micro-Renathane Tubing	Braintree Scientific	MRE025
Micro-Renathane Tubing	Braintree Scientific	MRE033
One Touch Ultra2 System Kit 1	One Touch	N/A
One Touch Ultra Blue Mail Order Test Strips, 50 CT	One Touch	020-963
Mouse/Rat Noradrenaline ELISA	Eagle Biosciences	NOU39-K01 0

RESOURCE AVAILABILITY

Lead Contact
Further information and requests for resources and reagents should be directed to and will be fulfilled by the Lead Contact, Amber L. Alhadeff (aalhadeff@monell.org).

Materials Availability
This study did not generate new unique reagents.

Data and Code Availability
The published article includes all datasets generated or analyzed during this study. Detailed datasets and codes supporting the current study are available from the lead contact upon request.

EXPERIMENTAL MODEL AND SUBJECT DETAILS

Mice were group housed on a 12:12 h light/dark cycle in a room set to 72°F with *ad libitum* access to food (LabDiet Rodent 5001) and water unless noted otherwise. Adult (at least 8 weeks old) male and female mice were used for experiments. *Agrp-IRES-Cre* (Jackson Labs 012899, *Agrp$^{tm1(cre)Lowl}$/J*) (Tong et al., 2008) and C57BL/6J mice were used. *Agrp-IRES-Cre* mice were purchased from Jackson and bred and genotyped to generate experimental animals. C57BL/6J mice were imported from Jackson and used for experimentation. All mice were habituated to handling and experimental conditions prior to experimentation. For within-subject analyses, mice received all experimental conditions in a counter-balanced fashion. For between-subject analyses littermates were randomly assigned to experimental condition. Both male and female mice were used, and we did not observe any significant sex differences. We therefore combined results obtained from male and female mice to ensure the studies were sufficiently powered and minimize the number of animals needed. All procedures were approved by the Monell Chemical Senses Center and University of Pennsylvania Institutional Animal Care and Use Committees.

METHOD DETAILS

Recombinant Adeno-Associated Virus (rAAV)
AAV1.Syn.Flex.GCaMP6s.WPRE.SV40 (titer: 4.216e13 GC/mL, Addgene 100845) was used to monitor calcium activity in AgRP neurons. CAG, promoter containing a cytomegalovirus enhancer; the promoter, first exon and first intron of the chicken beta actin gene; and the splice acceptor of rabbit beta-globin gene. Syn, human Synapsin 1 promoter. Flex, Cre-dependent flip-excision switch. WPRE, woodchuck hepatitis virus response element. GCaMP, Genetically encoded calcium indicator resulting from a fusion of GFP, M13 and Calmodulin.

Viral Injections and Fiber Optic Implantation
Mice were pretreated with subcutaneous injections of meloxicam (5 mg/kg, Norbrook Laboratories, 55529-040-11) and bupivacaine (2 mg/kg, Moore Medical, 52683) and anesthetized in an induction chamber with isoflurane (1.5%–3%, Clipper, 0010250). Mice were placed in a stereotaxic frame and intracranial viral injections were performed as previously described (Alhadeff et al., 2018; Su et al., 2017). For fiber photometry experiments, unilateral injections of GCaMP6s (300 μL of virus) were performed in the arcuate nucleus of the hypothalamus (1.35 mm posterior to bregma, 0.25 mm lateral to midline, and 6.15-6.3 mm ventral to skull). A ferrule-capped optical fiber (400 μm core, NA 0.48, Doric, MF2.5, 400/430-0.48) was implanted 0.2 mm above the injection site and secured to the skull with Metabond cement (Parkell, S380) and dental cement (Lang Dental Manufacturing, Ortho-jet BCA Liquid, B1306 and Jet Tooth Shade Powder, 143069). Experiments took place at least 2 weeks following surgery to allow for recovery and viral expression.

Cell Metabolism
Short Article

CellPress

Gastric/Intestinal Catheter Implantation

Mice were treated with meloxicam (5 mg/kg), bupivacaine (2 mg/kg) and buprenorphine (1 mg/kg) analgesia subcutaneously. Mice were anesthetized with isoflurane (3%) in an induction chamber and then transferred to a sterile drape while maintaining continuous isoflurane (1%–2%) administration through a nose cone. An abdominal midline incision through the skin and muscle was performed. For gastric catheters, Micro-Renathane catheter tubing (7 cm length, Braintree Scientific, MRE-033) with epoxy balls on each end (Devcon Clear Epoxy Adhesive, 92926, Lowes) was inserted into the fundus of the stomach through a puncture hole. For intestinal catheters, Micro-Renathane catheter tubing (7 cm length, Braintree Scientific, MRE-025) was used. The catheter was inserted ~5 mm distal to the pylorus (duodenum) or ~5 mm proximal to the cecum (ileum). All catheters were secured to the tissue with surgical mesh (5 mm diameter piece, Bard, 0112660). The unsecured end of the catheter was guided through an intrascapular incision and secured with surgical mesh and suture. The catheter was flushed with sterile water and sealed with a metal cap after surgery to prevent blockage. Mice were provided moistened chow and given at least 2 weeks to recover from surgery. Post-operative body weights were recorded daily to ensure pre-surgical weights were reached prior to starting experiments.

Hepatic Portal Vein Catheter (HPV) Implantation

HPV catheters were assembled using Micro-Renathane catheter tubing (8 cm length, Braintree Scientific, MRE-025). About 1.5 cm of the tip was tapered to 0.35-0.4 mm OD by pulling in 160°C mineral oil, and beveled to a ~60° angle. The tubing was attached to a 12 mm long 26-gauge V-shaped cannula and secured with a few drops of cyanoacrylate glue (Loctite 4061). The cannula was attached to an oval piece of Premilene Mesh (ca. 1.2cm^2, no. 1064435; B. Braun Surgical S.A. Rubi, Spain) with monofil suture (4/0 Braunamid white no. 118503/9; B. Braun, Germany). Prior to surgery, catheters were sterilized, rinsed well, and filled with sterile saline.

Mice were anesthetized and treated with analgesia as described above. An intrascapular incision was made and the infusion port was placed subcutaneously between the scapulae. An abdominal incision was made through the skin and muscle and the catheter was guided subcutaneously to the abdominal incision. The HPV was exposed and a small puncture hole was made into the superior mesenteric vein about 9 mm upstream of the HPV using a tapered suture needle tip (from Prolene 4-0, Ethicon 8881). The tip of the catheter was immediately inserted 4-5 mm into the vein so that the tip was at least 3 mm upstream of the gastroduodenal vein. The catheter was fixed in place with 8/0 prolene suture (Ethicon EH7470), filled with a heparinized (200 IU heparin/mL, Midwest Vet, 191.46750.3) 50% glycerol (Sigma-Aldrich, G7893-600ML) solution, and sealed with a metal cap. Mice were given moistened chow and allowed at least 2 weeks to recover from surgery and regain pre-surgical body weight. Catheters were flushed with sterile saline and the glycerol solution was replaced every 3-4 days.

Complete Subdiaphragmatic Vagotomy

Mice were maintained on a liquid diet (Ensure Plus Vanilla, Abbott, 53642) for at least 3 days prior to surgery to promote survival. Mice were anesthetized and treated with analgesia as described above and an abdominal midline incision was made through skin and muscle. The stomach was laparotomized to expose the esophagus, and the dorsal and ventral vagal trunks were exposed and isolated from the esophagus. The vagal trunks were resected and cauterized as we have previously published (Alhadeff et al., 2019). A pyloroplasty was then performed by making a small incision across the pyloric sphincter and suturing the incision to widen the sphincter and promote survival (Dezfuli et al., 2018). Finally, a gastric catheter was implanted as described above. Control mice received a sham surgery that consisted of all surgical procedures (including pyloroplasty) except for the resection and cauterization of the vagus nerve.

Celiac-Superior Mesenteric Ganglionectomy

Splanchnic afferents course through the pre-vertebral celiac and superior mesenteric ganglia. Therefore, to determine splanchnic contributions to gut-brain nutrient sensing, we monitored *in vivo* neural activity AgRP neurons in mice following celiac-superior mesenteric ganglionectomy (CSMG) (Bohland et al., 2014; Fujita and Donovan, 2005; Sclafani et al., 2003). Mice were anesthetized and treated with analgesia as described above. An abdominal midline incision was made through skin and muscle. The aorta was exposed at the branching site of the celiac and superior mesenteric arteries, just medial to the left kidney. The celiac and superior mesenteric ganglia and tissue surrounding the three blood vessels were gently teased away with forceps until the area between them was clear of nerve and lymphatic tissue. Sham animals underwent the same procedures but the ganglia were left intact. Mice were given at least 1 week to recover and their weights were recorded daily to ensure they returned to pre-surgical body weights before experimentation. In addition to visual verification of CSMG during surgery, we verified the success of the surgery post hoc by analyzing intestinal norepinephrine levels, as the celiac and superior mesenteric ganglia are the main sources of norepinephrine in the stomach and intestine (Li et al., 2010). Intestinal tissue (50 mg) was homogenized in the presence of 0.01 M HCl, 0.15 mM EDTA, and 4 mM sodium metabisulfite and centrifuged for 15 min at 15,000 rcf. The supernatant was collected and used for ELISA analysis (Eagle Biosciences, NOU39-K10; Riera et al., 2017) according to manufacturer's instructions.

Food Restriction

Mice were singly housed during experimentation and their food was restricted to maintain 85%–90% of their free-feeding body weight. Mice were weighed at the same time each day and given a chow aliquot (1.5-3.0 g, taking into account any calories

consumed/infused during experiments) after experimentation to maintain their body weight. For food deprivation, food was removed from the cage 24 h prior to the start of experiments.

Dual-wavelength Fiber Photometry (FP)

Dual-wavelength FP was performed as we and others have previously described (Lerner et al., 2015; Su et al., 2017; Zalocusky et al., 2016). Both 470-nm and 405-nm excitation wavelengths were used simultaneously in each subject. 470 nm excites calcium-dependent GCaMP6s fluorescence providing a proxy for neural activity. 405 nm excites calcium-independent fluorescence and serves as a control for movement and bleaching artifacts. Excitation lights were generated through fiber-coupled LEDs (Thorlabs, M470F3 for 470 nm and M405F1 for 405 nm) and modulated by a real-time amplifier (Tucker-Davis Technology, RZ5P) at 211 and 566 Hz for 470 and 405 nm, respectively. Excitation lights were passed through bandpass filters (Thorlabs, MF469-35 for 470 nm and FB405-10 for 405 nm) before being collimated and combined by a 425-nm long-pass dichroic mirror (Thorlabs, DMLP425). The combined excitation light was delivered through a 400-μm core, 0.48 NA, low-fluorescence optical fiber (Doric, MFP_400/430/1100-0.48_1.5_FCM-MF). The patch cord was connected to an implanted fiber (Doric, MFC_400/430-0.66_6.5mm_MF2.5_FLT). The patch cord and 2.5-mm diameter ferrule containing the fiber were secured using an interconnector (Thorlabs, ADAF2). GCaMP6s emission fluorescence signals were collected through the same patch cord, collimated, passed through a GFP emission filter (Thorlabs, MF525-39), and focused onto a femtowatt photoreceiver (Newport, Model 2151, gain set to DC LOW) using a lens (Edmund Optics, 62-561). The emission signals were converted to electrical signals, sampled at 1017 Hz, and demodulated by the RZ5P real-time processor. LEDs were externally controlled by Synapse (Tucker-Davis Technology). Synchronized infra-red cameras (Ailipu Technology, ELP-USB100W05MT-DL36) were used to video-record mice during experiments.

Experiments were performed as previously described (Alhadeff et al., 2019; Su et al., 2017). All experiments were performed in the subject's home cage with the lid removed following habituation to procedures and tethering. GCaMP6s fluorescence signals were set to similar levels by adjusting the 470- and 405-nm LED output power. GCaMP6s fluorescence was recorded for 5-min prior to delivery of the stimulus (infusion, injection, etc.) and used as the baseline signal for analyses as described below.

Fiber Photometry Inclusion Criteria

1-2 weeks following surgery, mice were food-deprived overnight and their AgRP neuron activity was monitored. Following a 5-min baseline, a chow pellet was presented to the animal and their neural activity was monitored for 10 min following food delivery. Mice that had < 20% ΔF/F were excluded from experiments.

Fiber Photometry Recordings During Gastrointestinal Infusions

Mice were habituated to fiber photometry and catheter handling prior to experiments. Following a 5-min baseline, food restricted mice were infused with 1 mL of infusate in a counterbalanced experimental design unless specified otherwise. Catheters were connected to tubing and a syringe placed into an infusion pump (Harvard Apparatus, 703007). Infusions were performed at a rate of 0.1 mL/min (Alhadeff et al., 2019; Han et al., 2016; Su et al., 2017). Catheters were flushed with sterile water before and after experiments to prevent clogging.

Glucose, fat, amino acids, and Ensure Plus were dissolved or diluted in sterile water to 1/3-1 kcal/mL. NaCl (1.8% and 2.7%), MDG (8%), urea (5.6%), 3-oMG (8% and 16%) and mannitol (8% and 16%) were dissolved in sterile water. To verify vagotomy, 30 μg/kg CCK (Bachem 4033101) was dissolved in saline and injected i.p. To inhibit SGLT1/3, 0.4% phlorizin (Tocris, 4627) was dissolved in an 8% glucose solution. To inhibit GLUT2, 0.23% phloretin (Sigma, P7912) was dissolved in an 8% glucose solution. 3.25% NaOH was added to both phlorizin and phloretin solutions to ensure they were fully dissolved (Zukerman et al., 2013). To control for effects of NaOH on AgRP neuron activity, these infusions were compared to vehicle solution containing 3.25% NaOH in glucose. To block fat digestion, 4 or 250 mg orlistat (Sigma, O4139) per g of fat was added to 1 kcal/mL Intralipid. Drug doses were selected based on prior demonstration of these inhibitors' ability to alter post-ingestive effects on feeding behavior (Sclafani and Ackroff, 2018; Zukerman et al., 2013). Oleic acid was diluted to 12.5% in 1.5% TWEEN 80 in PBS and was sonicated to emulsify.

Fiber Photometry Recordings During HPV Infusions

30 min prior to FP recordings, the heparinized glycerol solution was aspirated from the catheter and the catheter was flushed with sterile saline. The catheter was then filled with 6% trisodium citrate (Sigma, S1804) to prevent clogging of the catheter before the start of experiments. Experiments took place as described above, but with an infusion rate of 50 μL/min for a total infusion volume of 500 μL. Glucose (10% and 20%), Intralipid (8%), NaCl (0.9%, 1.8%, and 3.6%), urea (6.7%), 3-oMG (20%), and KCl (2.2%) solutions were prepared as described above and sterilized prior to infusions. Following experiments, catheters were again flushed with sterile saline and filled with heparinized 50% glycerol.

Fiber Photometry Data Analysis

Data were exported from Synapse to MATLAB (MathWorks) using a script provided by Tucker-Davis Technology. Custom MATLAB scripts were used to independently process and normalize 470- and 405-nm signals to baseline signals. ΔF/F was calculated as $(F-F_{baseline})/F_{baseline}$, with $F_{baseline}$ being the median of 5-min pre-stimulus signal. Data were down-sampled to 1 Hz. The subsequent analysis of FP data was performed in MATLAB. Mean ΔF/F was calculated by integrating ΔF/F over a period of time and then dividing by the integration time. Minimum and maximum ΔF/F were calculated by taking the 10 s mean ΔF/F for each mouse at the average

Cell Metabolism
Short Article

 CellPress

minimum or maximum of each recording. Time to 50% of minimum ΔF/F was calculated by identifying the first time point at which the ΔF/F of a mouse reached 50% of the individual minimum ΔF/F for that mouse.

Food Intake Experiments
Mice were habituated to a home cage lined with a KimTech bench protector. On the day of experimentation, food restricted mice were infused with water, NaCl, glucose, Intralipid, or amino acids (1 mL, 0.1 mL/min) diluted in water to 1/3 kcal, 2/3 kcal, or 1 kcal as described above. In separate experiments, food restricted mice were infused with oleic acid or its vehicle, or Intralipid/orlistat or Intralipid. After infusion, all mice were provided with a weighed pellet of chow and intake was measured manually at 30 min following infusion, accounting for crumbs. Mice had *ad libitum* access to water during experiments.

Blood Glucose Measurements
Mice were food deprived 24 h prior to experiments. Blood glucose levels were measured before and after IP injections of glucose and equi-osmotic NaCl. The tip of the mouse's tail was cut and a drop of blood collected onto a blood glucose monitor (OneTouch Ultra2) to determine baseline blood glucose levels. Mice were then injected IP with glucose (2 g/kg, 10 μL/g of body weight) or the same volume of 4.14% NaCl in a counter-balanced design. Blood was again collected and measured 10 min after the injection.

Histology and Imaging
After the completion of experiments mice were deeply anesthetized with isoflurane (Clipper, 0010250) and transcardially perfused with 0.1 M Dulbecco's phosphate-buffered saline (PBS, HyClone, SH30013.04) followed by 4% paraformaldehyde (MP Biomedicals, 150146). Brains were post-fixed overnight in 4% paraformaldehyde then transferred to PBS. 200-μm coronal sections were prepared with a vibrating blade microtome (Leica, VT1000S). Epifluorescence images were taken on a Leica SPE microscope to verify viral expression and fiber placements.

QUANTIFICATION AND STATISTICAL ANALYSIS

Data were expressed as means ± SEMs in figures and text. Paired or unpaired two-tailed t tests were performed as appropriate. One-way, two-way, and repeated-measures ANOVA were used to make comparisons across more than two groups using Prism 8 (Graph-Pad), and normality was tested using the Kolmogorov-Smirnov test. Test, statistics, significance levels, and sample sizes for each experiment are listed in Tables S1 and S2. ns $p > 0.05$, t tests and post hoc comparisons: $^{*}p < 0.05$, $^{**}p < 0.01$, $^{***}p < 0.001$; interaction: $\infty p < 0.05$, $\infty\infty p < 0.01$, $\infty\infty\infty p < 0.001$; main effect (group, condition or drug): $\diamond p < 0.05$, $\diamond\diamond p < 0.01$, $\diamond\diamond\diamond p < 0.001$.